Chapter 3

Robust Color Image Restoration

Conventional image restoration problem is well addressed in literature. However, robust, blind and color image restoration are comparatively less studied subjects. As the central idea of image restoration is still the same, we will view the general ideas proposed in the literature. Our survey is not from a historic perspective, but the one which is related to our proposed work. A few of the authors [5, 6, 39, 59, 117] classify restoration problem as linear, non-linear, iterative, non-iterative, deterministic, probabilistic, model-based etc. We review some of the iterative algorithms.

In general, image restoration algorithms can be classified mainly on the basis of pre-determined criteria used to achieve a good estimate of the image. These algorithms can be viewed as variants of the following approaches:

1. Optimality criterion
2. Constrained optimality criterion, and
3. Feasibility criterion

This chapter is organized as follows: In sections 1-3 we discuss the above mentioned methods, as a literature review The proposed robust color image restoration is discussed in section 4. Section 5 summarizes this chapter.

3.1 The Optimality Criterion

Consider the image restoration problem (without noise) as given in Eqn. (1.2) $Y = \mathbf{H}X$. If the inverse of the PSF $\mathbf{H}$ exists, and is denoted as $\bar{\mathbf{H}}$, then the estimate of the actual

image X can be obtained as

$$\hat{X} = \bar{\mathbf{H}}Y \tag{3.1}$$

In the presence of noise, estimate will contain undesirable frequencies [6]. Moreover, in most of the restoration problems, inverse of the PSF does not exist [6, 105]. To circumvent this problem, an estimate of the image is obtained by computing a pseudo inverse or the generalized inverse of the PSF matrix, with the underlying principle being to estimate the image as a minimum of the function

$$\|Y - \bar{\mathbf{H}}X\|_2^2 \tag{3.2}$$

where, $\|.\|_2$ is the Euclidian norm.
From Eqn. (3.2), we deduce the estimate of the image as:

$$\hat{X} = (\mathbf{H}^T\mathbf{H})^{-1}\mathbf{H}^T Y. \tag{3.3}$$

This is the conventional l_2 approach. The pseudo inverse of $\mathbf{H}$ can be calculated using single value decomposition [38].

Conventional l_2 approaches are noise sensitive [105] and ignore noise information completely while estimating the solution, but make use of the complete information about the PSF. These methods unnecessarily square the conditional numbers making the system unstable [6]. To overcome the noise problem, a truncated singular expansion has been suggested by Sullivan and Katsaggelos [135]. Also, the l_2 approach may result in a negative image, even though the original one was non-negative.

3.2 Constrained Optimal Methods

-

The main focus of these approaches is to estimate the image by satisfying constraints on the solution space. Effectively, it uses *a priori* information about the original image [105]

3.2.1 Constrained l_2 Approach

This approach belongs to the class of well-known regularization method suggested by Tikhonov [137, 136]. This approach imposes a degree of smoothness on the solution of the l_2 problem. It can be formulated in two different ways [5, 49]

1. *First kind:*

$$\begin{array}{c} min \;\; X^T S X \\ subjected \;\; to \;\; (Y - \mathbf{H}X)^T W (Y - \mathbf{H}X) = e \end{array} \tag{3.4}$$

where, S is a non-negative definite matrix, W is an error weighting matrix and e is the residual error. Constrained l_2 solution, $\hat{X}_{l_2}$ for the above equation is:

$$\hat{X}_{l_2} = (H^T W^{-1} H + \frac{1}{\lambda_l} S)^{-1} H^T W Y \tag{3.5}$$

where λ_l is a parameter, chosen to satisfy a compromise between residual error and smoothness in the estimate [137, 136].

2. *Second kind:*

$$\begin{array}{c} min \;\; (Y - \mathbf{H}X)^T W (Y - \mathbf{H}X) \\ subject \;\; to \;\; X^T S X = d_s \end{array} \tag{3.6}$$

with d_s denoting the degree of smoothness. Solution is then

$$\hat{X}_{l_2} = (H^T W^{-1} H + \gamma_l S)^{-1} H^T W Y \tag{3.7}$$

where γ_l is a Lagrangian multiplier.

The solutions in Eqn. 3.5 and Eqn. 3.7 will be the same, if $\lambda_l = 1/\gamma_l$. The need to estimate the values of S, λ_l and γ_l is the drawback of these techniques, as it is a difficult problem [42, 146].

3.2.2 Maximum Entropy Method

This is a non-linear estimation technique. In order to overcome the possibility of a negative solution in the conventional l_2 approach, the maximum entropy methods are suggested [6, 32]. Using the entropy as the measure of uncertainty, algorithms have been developed to solve:

$$\begin{array}{c} max \;\; (-\sum_{i=1}^{M} \sum_{j=1} M x_{i,j} \log(x_{i,j})) \\ subject \;\; to \;\; \frac{1}{2}\|Y - \mathbf{H}X\| = \sigma_r^2, \quad \sum_{i=1}^{M} \sum_{j=1} M x_{i,j} = 1 \end{array} \tag{3.8}$$

where σ_r^2, greater than zero, is pre-specified. Since $x_{i,j} \geq 0$, the normalized sum

$$\sum_{i=1}^{M} \sum_{j=1} M x_{i,j} = 1 \tag{3.9}$$

can be viewed as a probability distribution whose entropy is the objective function of Eqn. (3.9). The implicit solution of (3.8) can be expressed as

$$\hat{X} = \exp\{-1 - \lambda_l \mathbf{H}^T (Y - \mathbf{H}\hat{X})\} \tag{3.10}$$

where $\exp(z)$ is a vector consisting of elements $\exp(z_{i,j}), i, j = 1, 2 \ldots M$ and λ_i is the Lagrangian multiplier.

3.2.3 Bayesian Approach

The methods presented earlier assume a linear model. Non-linear models were suggested by Pvlovic and Trussel [103], Hunt [50] and Trussel [139]. The Bayesian approach suggested in these gives us flexibility in incorporating *a priori* knowledge and also in handling multiplicative and signal dependent noise. Here, the actual image x and observed image y are treated as random vectors. The image estimate x_{MAP} (MAP - Maximum *a posteriori*) is obtained by maximizing the posterior conditional density functions [50],

$$\max_x P[X = x|Y = y] \tag{3.11}$$

This method can make use of any *a priori* knowledge like noise characteristics.

Under Gaussian assumption on x, Hunt [50] has showed that the gradient ascent/descent techniques have very slow convergence. Later, Trussel and Hunt [140] proposed an improved method based on the use of the variance of the residual information.

Geman and Geman [36] suggested a MAP estimation approach using Gibbs distribution. It finds an estimate of the actual image from the degraded image, which has undergone blurring and is corrupted by noise. Apart from this, they provided a mechanism to estimate the image such that the discontinuities are also preserved. For actual implementation, they suggested the simulated annealing (SA) algorithm [73]

Several other approaches such as mean field annealing [37], neural networks [2, 31, 128] etc. have been suggested in the literature, for faster convergence. Geman and Reynolds [35] also suggest a non-linear filtering method to solve the problem.

3.2.4 Minimum Mean Square Error(MMSE)

The stochastic approaches suggested in the signal processing literature have been extended to solve image restoration problem [6, 59]. A few of them are discussed here.

Assuming the original image as a realization of a Gaussian random process, with known first and second order statistics, the Wiener filter [6, 49, 59] has been shown to minimize the mean square estimation error

$$E[(x - \hat{x})^T(x - \hat{x})] \tag{3.12}$$

where, $\hat{x}$ is the estimate of x. Different approaches for this method are compiled by Sezan [126].

Another well-known approach in the stochastic filtering domain is the Kalman filter [56, 60, 150]. This is a state-space approach and assumes the given image to be a Gauss-Markov random field, and an auto-regressive model,

$$x_{i,j} = \sum_{(k,l)\in\eta_c} c_{k,l} x_{i-k,j-l} + v_{i,j} \tag{3.13}$$

where η_c is the model support, $c_{k,l}$ is the model coefficient for $(k,l) \in \eta_c$ and $v_{i,j}$ is the modeling error. Then the Kalman filter estimates the image as a state vector, from the previous state of the system (recursively) [30, 108]. Different approaches in one and two dimensions are reported in [90]. To reduce computation as well as storage capacity, a reduced order model of the Kalman filter is reported in literature [5]. Several restoration techniques have been proposed in higher dimension state-space models to reduce the effective size of the vector [153].

3.3 Feasibility Criterion Approach

This method estimates the image as a candidate member of the set S. This set is formed by the intersection of a finite number of sets S_i, where each set S_i corresponds to some *a priori* knowledge of the actual image, the blurring function and noise. These methods vary in the way the constraints are used while restoring the image.

One of the methods is to use an iterative algorithm. The basic idea is: Find the set of an image x iteratively in the form

$$x(k+l) = C(x(k)) \tag{3.14}$$

where $x(0)$ is the initial estimate, and C is an operator defined using *a priori* information. The fixed point of the above iterative technique is considered as an estimate of the actual image. The primary requirements are that the operator C must be either contractive or non-expansive.

Most of the algorithms estimate the image when the precise knowledge of PSF is available. They work for space-invariant [13] as well as for space-variant blur [141].

Kundur [74, 75] and Banham [8] review some of the other popular techniques for image restoration.

3.4 The Proposed Method: Restoration of Multichannel Images

This section deals with the restoration of colored images, distorted by both intra- and inter-channel blur, and corrupted by additive white Gaussian noise. The image is modeled as a Markov Random Field (MRF), and color image restoration is cast as a maximum *a posteriori* (MAP) estimation problem. We propose a First Order Interchannel Interaction (FOII) model for image restoration. Simulated annealing algorithm is then used to minimize the posterior energy function. We compare the simulation results of conventional non-interaction (NI) approach and the proposed FOII approach. The simulation results show that FOII works better when interchannel degradation is considered. The proposed model is fairly general, and the results are satisfactory even when the interchannel degradation parameter is unknown.

The aim of image restoration is to recover the original image from a degraded image, corrupted by noise. Typically, degradation is modeled by a linear blur. Some sources of blur are motion blur, out-of-focus blur, atmospheric turbulence, and others. Noise may arise from digitization and quantization, transmission and recording medium, thermal noise, etc. Classical methods of image restoration [6, 66] assume the blurring operation is exactly known *a priori*. The observed image is then de-convolved using the known blurring function. This approach basically involves the solutions of an equation, which is usually ill conditioned [41]. This ill-conditioning is overcome by the regularization procedures [137].

Restoration of monochrome images, when the blurring function is known, is well addressed in literature [6, 66]. Some of the earlier techniques are complied by Sezan [126]. Recent developments are reported by Kundur *et al* [74, 75] and Banham *et al* [8] and the references therein. Results for color image restoration are not all that satisfactory mainly because, the psychology of color image perception in human beings is not fully understood.

It is assumed that the color planes do interact linearly with each other. Such models for color images have been reported in the literature. For example Panjwani *et al* [102] proposes such a model for color image segmentation.

In this section, we assume color planes interact linearly with each other. To account for the interchannel blurring, we propose a new model for interchannel interaction, namely, the First Order Interchannel Interaction (FOII) model. Then, a probabilistic approach is used by modeling the color image as a Markov Random Field (MRF). Restoration

problem is then cast as a maximum *a posteriori* (MAP) estimation problem. The choice of the energy function in the MRF model takes care of the dependencies between the color coordinates. In general, the energy function will be non-convex with multiple local minima and non-unique global minima. We use simulated annealing (SA) algorithm with inverse log-cooling schedule for energy minimization.

3.4.1 Image Model

To make this chapter relatively self sufficient, we give some of the important concepts of MRF again.

Let X be the lexicographically ordered (row transposed stacking) vector for an $M \times M$ image [6].

Definition 3.1 *X is a Markov random field if and only if*

$$P[X_{i,j} = x_{i,j} \mid X_{k,l} = x_{k,l}, \forall (k,l) \neq (i,j)] = P[X_{i,j} = x_{i,j} \mid X_{k,l} = x_{k,l}, (k,l) \in \eta_{i,j}] \tag{3.15}$$

Where $P[\ \mid\ ]$ is the conditional probability and $\eta_{i,j}$ is the neighborhood of (i,j). The neighborhood condition is translation independent except at boundaries, where a free boundary assumption is made.

Now, according to the Hammersely and Clifford theorem [9, 36], $P[X = x]$ can be written as:

$$P[X = x] = \frac{1}{Z} exp(-U(x)) \tag{3.16}$$

The normalizing constant Z (the partition function) is given by,

$$Z = \sum_{all\ config.x} exp(-U(x)) \tag{3.17}$$

and $U(x)$ is the (Gibbs) energy function, given by

$$U(x) = \sum_{c \in \mathcal{C}} V_c(x) \tag{3.18}$$

with $\mathcal{C}$ being the set of all *cliques* [36]. A typical unconditional problem would be to estimate a configuration x, such that $P[X = x]$ is maximized, or equivalently, $U(x)$ is minimized [23] (also see appendix B).

We extend the monochrome image observation model as given in [6] for the color image as:

$$Y = \phi(\mathbf{H}X \odot N) \tag{3.19}$$

where, Y is the observed image vector, X is the original image vector, $\mathbf{H}$ is the PSF matrix and N is the corrupting Gaussian noise vector which is assumed to be independent of X, $\phi(.)$ is an operator (possibly non-linear) and $\odot$ is an inervitable operation (for example, addition or multiplication). Note that for a color image of size $M \times M$, X, Y, N, all are lexicographical ordered column vectors of size $3M^2 \times 1$.

The structure of X is then,

$$X = [X_{0,0} \;\; X_{0,1} \ldots X_{M-1,M-1}]^T \tag{3.20}$$

where,

$$X_{i,j} = [x^r(i,j) \;\; x^g(i,j) \;\; x^b(i,j) \;\;]^T, \qquad 0 \;\leq\; i,j \;\leq\; M-1 \tag{3.21}$$

Superscripts r, g, b corresponds to red, green and blue color planes respectively. The structures of Y and N will be similar to that of X. $\mathbf{H}$ will be a $3M^2 \times 3M^2$ matrix, whose structure has similarity with, the one given by Bhat [12] for monochrome images. Precise structure of $\mathbf{H}$ will be,

$$\mathbf{H} = \begin{pmatrix} H_\xi & H_1 & H_1 & 0 & \ldots & H_1 & H_1 \\ H_1 & H_\xi & H_1 & H_1 & \ldots & 0 & H_1 \\ \vdots & \vdots & \vdots & \vdots & \ddots & \vdots & \vdots \\ H_1 & H_1 & 0 & \ldots & H_1 & H_1 & H_\xi \end{pmatrix} \tag{3.22}$$

where

$$H_\xi = \begin{pmatrix} \bar{H}_\xi & \bar{H}_1 & \bar{H}_1 & 0 & \ldots & \bar{H}_1 & \bar{H}_1 \\ \bar{H}_1 & \bar{H}_\xi & \bar{H}_1 & \bar{H}_1 & \ldots & 0 & \bar{H}_1 \\ \vdots & \vdots & \vdots & \vdots & \ddots & \vdots & \vdots \\ \bar{H}_1 & \bar{H}_1 & 0 & \ldots & \bar{H}_1 & \bar{H}_1 & \bar{H}_\xi \end{pmatrix} \tag{3.23}$$

$$\bar{H}_\xi = \begin{pmatrix} 1 & \xi & \xi \\ \xi & 1 & \xi \\ \xi & \xi & 1 \end{pmatrix} \tag{3.24}$$

and $\bar{H}_1$ is:

$$\bar{H}_1 = \begin{pmatrix} 1 & 0 & 0 \\ 0 & 1 & 0 \\ 0 & 0 & 1 \end{pmatrix} \tag{3.25}$$

The structure of H_1 will be same as that of H_ξ with $\bar{H}_\xi$ replaced by $\bar{H}_1$ as given below:

$$H_1 = \begin{pmatrix} \bar{H}_1 & \bar{H}_1 & \bar{H}_1 & 0 & \ldots & \bar{H}_1 & \bar{H}_1 \\ \bar{H}_1 & \bar{H}_1 & \bar{H}_1 & \bar{H}_1 & \ldots & 0 & \bar{H}_1 \\ \vdots & \vdots & \vdots & \vdots & \ddots & \vdots & \vdots \\ \bar{H}_1 & \bar{H}_1 & 0 & \ldots & \bar{H}_1 & \bar{H}_1 & \bar{H}_1 \end{pmatrix} \tag{3.26}$$

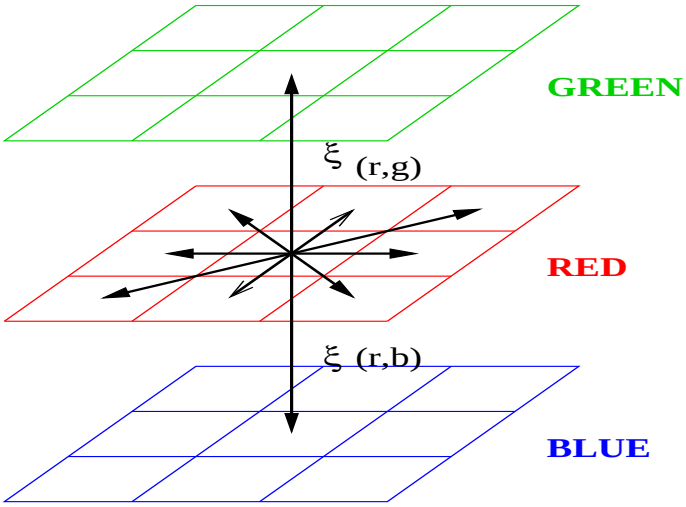

Figure 3.1: Interchannel Blurring Operation

The **H** matrix is appropriately normalized. *The term ξ decides the amount of interchannel blurring operation.* The Interchannel blurring is pictorially shown in Fig.3.1.
At the pixel level, the above model can be written (for red coordinate) as

$$y^r(i,j) = \sum_{(k,l)\in S} h(k,l)x^r(i-k,j-l) + \xi x^g(i,j) + \xi x^b(i,j) + n^r(i,j) \tag{3.27}$$

where S is the support of the point spread function (PSF) and superscript r implies the operation is for red color plane. Similarly y^g and y^b are defined for green and blue planes. We can generalize the model [Eqn.s (3.19) - (3.27)] by incorporating blurring degradation in other color planes [91]; for such a model, $\xi x^g(i,j)$ can be replaced by

$$\sum_{S_{rg}} h_{rg}(k,l)x^g(i-k)(j-l) \tag{3.28}$$

Such a model will be similar to that proposed by Panjwani and Healy [102].

Consider X and Y as defined in Eqn. (3.19); we assume that X is an MRF; thus X has the probability distribution given in Eqn. (3.16). With the color image observation model as described above, the color image restoration problem can be cast as:

Estimate X such that $P[X = x|Y = y]$ is maximized with respect to x.

Using Bayes rule, the *a posteriori* distribution can be expressed as

$$P[X = x|Y = y] = \frac{P[Y = y|X = x]P[X = x]}{P[y = y]} \tag{3.29}$$

Since Y is the observed image, $P[Y = y]$ is known. i.e., from Eqn. (3.19), we see that,

$$N = Y \ominus \phi HX. \tag{3.30}$$

Where, $\ominus$ is the inverse of $\odot$. The LHS of Eqn. (3.29) becomes,

$$P[Y = y|X = x] = P[N = Y \ominus \phi(HX)|X = x] \tag{3.31}$$

We further make the assumption:

- N with $N_{i,j} = [n^r\ n^g\ n^b]^T$ is is normally distributed with zero mean and covariance matrix $\sigma^2 I$ (I being a $3M^2 \times 3M^2$ identity matrix). Moreover, N is statistically independent of X.

Using the above assumption we have,

$$P[Y = y|X = x] = \frac{1}{(2\pi\sigma^2)^{M^2/2}} exp(-\frac{\|N\|_2^2}{2\sigma^2}) \tag{3.32}$$

where σ is the variance of the Gaussian noise, and

$$P[X = x] = \frac{1}{Z} exp\{-U(x)\} \tag{3.33}$$

Substituting Eqn.s (3.32) and (3.33) in Eqn (3.29) we get,

$$P[X = x|Y = y] = \frac{exp\{-U_p(x)\}}{(2\pi\sigma^2)^{M^2} Z K_e P[Y = y]} \tag{3.34}$$

with the *a posteriori* energy function given by [12]

$$U_p(x) = U(x) + \frac{\|n\|_2^2}{2\sigma_e^2} \tag{3.35}$$

In general, the *a priori* energy function $U(x)$ will have three color planes, as given in Eqn. (3.21), non-linearly interacting with each other. Moreover, to take care of discontinuities in the color planes, one could also incorporate horizontal and vertical line fields [36] corresponding to each color plane. Thus, the most general form for *a posteriori* energy function could be expressed as

$$U(x,h,v) = f(x^r, x^g, x^b, h^r, h^g, h^b, v^r, v^g, v^b)$$

where h^c and v^c represent horizontal and vertical line fields corresponding to the color plane c.

We propose two different forms for $U(x,h,v)$:

In the first form, we assume that the color planes c are uncorrelated. That is,

$$U_1(x,l,v) = \sum_{c=r,g,b} U_1(x^c, h^c, v^c) \tag{3.36}$$

and,

$$\begin{array}{ll} U_1(x^c,h^c,v^c) & = \sum_{i,j} \mu[(x^c_{i,j} - x^c_{i,j-1})^2(1-v^c_{i,j}) + (x^c_{i,j} - x^c_{i-1,j})^2(1-h^c_{i,j})] \\ & +\gamma[h^c_{i,j} + v^c_{i,j}] \;\; for \;\; c = r,g,b \end{array} \tag{3.37}$$

$l^c_{i,j} = 1(|x^c_{i,j} - x^c_{i-1,j}| - \theta^c_h)$ and $v^c_{i,j} = 1(|x^c_{i,j} - x^c_{i,j-1}| - \theta^c_v)$. θ's being the respective thresholds. μ is the smoothing parameter and γ provides penalty for every discontinuity. Function $1(z)$ is defined as:

$$1(z) = 1 \quad if \quad z > 0 \quad and \quad 0 \quad otherwise.$$

Term in the first bracket of the energy function Eqn. (3.37) signifies the interaction between the neighboring pixels. The second bracket term provides penalty for every discontinuity created and prevents spurious discontinuities. We call this model the non interaction (NI) model.

In the second form(FOII), we take into account first order interchannel interaction between color planes.

$$\begin{array}{ll} U_2(x,h,v) & = \sum_{i,j}\sum_c\sum_d \mu[(1-h^c_{i,j})(1-h^d_{i,j})(x^c_{i,j} - x^c_{i-1,j})(x^d_{i,j} - x^d_{i-1,j}) \\ & +(x^c_{i,j} - x^c_{i,j-1})(x^d_{i,j} - x^d_{i,j-1})(1-v^c_{i,j})(1-v^d_{i,j})] \\ & +\gamma[h^c_{i,j} + v^c_{i,j} + h^d_{i,j} + v^d_{i,j}] \quad for \;\; c,d \;\; = \;\; r,g,b \end{array} \tag{3.38}$$

Minimization of the *a posteriori* cost function can be done using a variety of minimization algorithms. We opt for the simulated annealing algorithm, as it guarantees convergence in probability.

3.4.2 Results

We report simulation results for the FOII energy functions given by (3.38) and compare its performance with the NI energy function given by (3.37). The original image was

degraded with different values of ξ, but during restoration, ξ was assumed to be 0, that is, *we do not have any knowledge of* ξ. For simulation purposes, we used a uniform, space invariant blur of size 5×5. White Gaussian noise was added (with $\sigma = 10$) separately on R,G and B. Reported here are the results for 64×64 checkerboard type synthetic and 128×128 Lisa images. Values of μ, γ and $\theta_l^c = \theta_v^c = \theta$ respectively were 0.025, 200.5 and 15 for the synthetic image and were 0.75, 150 and 20 respectively for the Lisa image. Stopping criterion for SA - was 1250 iterations for both images. Initial temperature was 5.15 and inverse log-cooling schedule was used. The value ξ selected is 0 (during restoration). All these parameters are selected such that we get acceptable results with both the methods.

To validate the performance, signal to noise ratio (SNR) of degraded and estimated images are computed as:

$$SNR = 10 \log \frac{\sum_{i,j} \|x(i,j)\|^2}{\sum_{i,j} \|x(i,j) - \hat{x}(i,j)\|^2}$$

with $\hat{x}$ being the estimated image. Results of simulation are tabulated. Few of the sample images are given at the end.

	Degraded image			NI			FOII		
ξ	R	G	B	R	G	B	R	G	B
0.4	14.77	14.64	15.05	16.31	16.99	15.10	20.15	17.28	17.82
0.6	14.65	14.51	14.91	18.78	16.28	16.45	20.15	17.28	17.82
0.8	14.57	15.68	16.07	18.88	18.88	19.46	19.89	20.44	21.42
1.0	14.36	15.37	15.80	17.73	18.45	19.29	19.38	19.97	20.72
1.25	14.14	15.19	15.66	17.53	18.17	18.10	18.71	19.44	19.29
1.5	14.12	15.14	15.65	17.09	17.82	17.85	18.30	18.89	19.33

Table 3.1: SNR Values for Synthetic image

3.4.3 Discussion and Conclusions

As can be seen from the tables 3.1- 3.2, the proposed FOII performs better than the NI model, for different values of ξ. Restored images are sharp and look better. Also, the model is robust to some extent, since we are able to obtain these results without any

	Degraded image			NI			FOII		
ξ	R	G	B	R	G	B	R	G	B
0.25	23.77	19.95	20.35	24.45	20.52	20.97	24.75	20.78	21.02
0.5	23.41	18.98	19.92	24.14	20.41	20.98	24.65	20.56	21.23
0.75	23.60	19.75	19.99	23.88	20.41	20.96	24.41	20.62	21.07
1.0	23.22	19.70	19.92	23.36	20.37	20.80	23.96	20.50	20.84
1.25	22.93	19.34	19.68	23.14	20.16	20.72	23.54	20.24	20.64
1.5	22.50	19.20	20.07	22.69	19.79	20.16	20.67	20.43	20.56

Table 3.2: SNR Values for Lisa image

knowledge of ξ. Performance of NI and FOII were found similar if $\xi = 0$ during blurring, which is expected.

The proposed model also worked satisfactorily when degradation was done in other color coordinates. For example, we degraded linearly in the YIQ and Ohta's [101] (also see appendix A) I_1, I_2, I_3 coordinates, and then transformed the resulting image to RGB domain. This will effectively do the interchannel blurring with unknown ξ. Encouraging results were obtained with FOII model. These results are reported in [70] and reproduced here:

Methodology.	R	G	B
Degraded Img.	14.30	15.36	15.79
Linear	16.03	17.71	18.13
FOII	17.79	19.09	19.74

Table 3.3: Synthetic image degraded in Ohta's coordinates

Methodology.	R	G	B
Degraded Img.	14.45	15.57	16.07
Linear	17.26	18.25	18.79
FOII	19.19	21.22	20.94

Table 3.4: Synthetic image degraded in YIQ coordinates.

From the tables (3.5 - 3.4) we see that the SNR values are comparable to the ones given in the previous tables (3.1 - 3.2). Thus, the FOII model seems to be fairly general, independent of the value of ξ

However, the proposed model is not an optimal one. SNR improvements are not all that satisfactory for highly textured images (Mandrill image, for example). This may be

due to the fact that some of the informations may be irrecoverably lost because of the 5×5 blur. However, for comparatively smooth image (faces, for example) the proposed algorithm does satisfactorily.

Figure 3.2: Lisa image: (left) Original, (right) Degraded in YIQ coordinates.

Figure 3.3: Simulation Results - Lisa image: (left) NI resorted, (right) FOII restored.

Figure 3.4: Sample synthetic images (left) Original, (right) Degraded in Ohta coordinates.

3.5 Summary

Image restoration is typically an ill-posed problem, which needs regularization. Regularization generally imposes smoothness constraints, which smooths the edges. To avoid

Methodology.	*R*	*G*	*B*
Degraded Img.	22.72	19.90	19.01
Linear	23.51	21.22	21.57
FOII	24.42	23.18	22.94

Table 3.5: Lisa image degraded in Ohta's coordinates

Methodology.	*R*	*G*	*B*
Degraded Img.	22.93	20.51	20.86
Linear	23.63	21.58	22.12
FOII	24.47	23.32	23.08

Table 3.6: Lisa image degraded in YIQ coordinates.

Restored Images

Figure 3.5: Restored synthetic images: (left) NI model (right) FOII model.

Figure 3.6: Synthetic image (left) degraded in YIQ coordinate (middle) Restored using NI and (right) Restored using FOII method.

Original

Degraded $\xi = 1.5$

Restored Images

NI

FOII

Figure 1: Simulation Results Lisa image

Results for $\xi = 0.8$

Original

Degraded

Restored Images

NI

FOII

Results for $\xi = 0.6$

Original

Degraded

Restored Images

NI

FOII

Figure 2: Simulation Results synthetic image

smoothing, line field based model was proposed in MRF domain. We model the image as an MRF and include line fields. Novelty of proposed model is that it takes into consideration the interaction of all color planes. This feature makes the proposed method to restore color images that have undergone interchannel blurring. It is shown that the proposed model works well even when the amount of interchannel degradation is unknown; thereby it can be termed as partially blind image restoration. Simulated annealing, which guarantees convergence to solution, is used to minimize the cost function. This slows down the convergence. Proposed model is not optimal; in the sense that, there is no significant improvements for a specific class of images. This class include images having high spatial frequency. For images with low spatial frequencies, proposed model works satisfactorily, both numerically and visually.